NANO LETTERS

Letter

pubs.acs.org/NanoLett

Rh-Doped Pt–Ni Octahedral Nanoparticles: Understanding the Correlation between Elemental Distribution, Oxygen Reduction Reaction, and Shape Stability

Vera Beermann,[†] Martin Gocyla,[‡] Elena Willinger,[§] Stefan Rudi,[†] Marc Heggen,[‡] Rafal E. Dunin-Borkowski,[‡] Marc-Georg Willinger,[§] and Peter Strasser*,[†]

[†]Electrochemical Energy, Catalysis, and Material Science Laboratory, Department of Chemistry, Technical University Berlin, 10623 Berlin, Germany

[‡]Ernst-Ruska Centre for Microscopy and Spectroscopy with Electrons and Peter Grünberg Institute, Forschungszentrum Jülich GmbH, 52425 Jülich, Germany

[§]Department of Inorganic Chemistry, Fritz-Haber-Institut der Max-Planck-Gesellschaft, Faradayweg 4-6, 14195 Berlin, Germany

Supporting Information

ABSTRACT: Thanks to their remarkably high activity toward oxygen reduction reaction (ORR), platinum-based octahedrally shaped nanoparticles have attracted ever increasing attention in last years. Although high activities for ORR catalysts have been attained, the practical use is still limited by their long-term stability. In this work, we present Rh-doped Pt–Ni octahedral nanoparticles with high activities up to 1.14 A mg_{Pt}^{-1} combined with improved performance and shape stability compared to previous bimetallic Pt–Ni octahedral particles. The synthesis, the electrocatalytic performance of the particles toward ORR, and atomic degradation mechanisms are investigated with a major focus on a deeper understanding of strategies to stabilize morphological particle shape and consequently their performance. Rh surface-doped octahedral Pt–Ni particles were prepared at various Rh levels. At and above about 3 atom %, the nanoparticles maintained their octahedral shape even past 30 000 potential cycles, while undoped bimetallic reference nanoparticles show a complete loss in octahedral shape already after 8000 cycles in the same potential window. Detailed atomic insight in these observations is obtained from aberration-corrected scanning transmission electron microscopy (STEM) and energy dispersive X-ray (EDX) analysis. Our analysis shows that it is the migration of Pt surface atoms and not, as commonly thought, the dissolution of Ni that constitutes the primary origin of the octahedral shape loss for Pt–Ni nanoparticles. Using small amounts of Rh we were able to suppress the migration rate of platinum atoms and consequently suppress the octahedral shape loss of Pt–Ni nanoparticles.

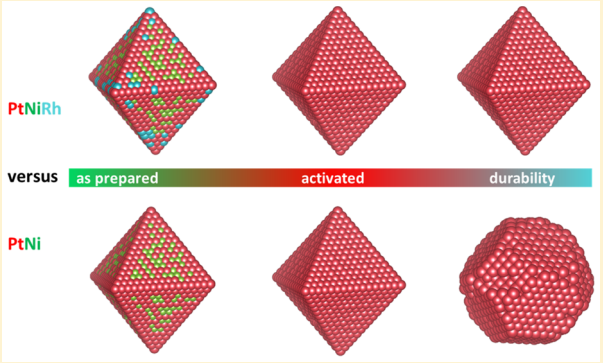

KEYWORDS: *oxygen reduction reaction, anisotropy, Rh-doped, octahedral nanoparticles, PtNi alloy, stability*

The urgent need of clean and renewable energy sources for transportation vehicles, portable devices and a variety of several other applications, triggered an intense research in polymer electrolyte membrane fuel cells (PEMFCs) in the last decades.[1] Pt and Pt-based nanoparticles supported on carbon are currently the benchmark catalysts for PEMFCs in the most industrial-related applications. However, due to the high costs caused by the amount of expensive Pt and the sluggish oxygen reduction activity of bimetallic Pt catalysts newly designed electrocatalysts for oxygen reduction reaction (ORR) based on Pt are required. The use of a 3d transition metal reduces the costs of a potential catalyst and improves the ORR rate by tuning the d-band structure of the Pt surfaces.[2,3] Several alloys of Pt with other transition metals such as Fe, Co, Ni, or Cu have been already discussed in literature.[4−8] As the ORR is a structure sensitive reaction, the surface structure of a catalyst is also an important parameter that needs to be considered. For spherical Pt nanoparticles in aqueous $HClO_4$ electrolyte, the specific activities are known to increase in the order of Pt(100) ≪ Pt(111) ≈ Pt(110), while for Pt–Ni alloys the order changes to (100) < (110) ≪ (111).[9] In 2007, Stamenkovic et al. demonstrated the different characteristics of certain Pt and Pt_3Ni single crystal surfaces and their high ORR activities that stimulated the intensive research on octahedral Pt–Ni nanoparticles enclosing (111) surfaces. In 2010, Zhang et al. described a successful synthesis of Pt_3Ni nanocubes and octahedra and compared the activities in terms of their (110)

Received: November 13, 2015
Revised: January 19, 2016
Published: February 8, 2016

DOI: 10.1021/acs.nanolett.5b04636
Nano Lett. 2016, 16, 1719–1725

and (111) surface structures.[10] Three years later the group of Xia was able to achieve Pt−Ni octahedral nanoparticles with a "record breaking" activity of 3.3 A mg_{Pt}^{-1} for the ORR using a similar method.[11,12] Another synthesis for Pt−Ni octahedral nanoparticles was introduced by Cui et al., who used a DMF-based solvothermal method. The particles resulting from this method also exhibit an exceptional high activity for ORR.[13,14]

Nevertheless, one considerable problem is still remaining: the limited long-term stability of Pt−Ni octahedral particles, which is due to the loss of their octahedral shape after a certain number of electrochemical cycles. For industrial applications, an improved long-term active and stable catalyst, which fulfills various requirements such as an initial high activity, a small activity drop during the lifetime of the catalyst, and a corresponding shape stability, is indispensable. However, only very few efforts have been made to overcome this problem.

Trimetallic octahedral nanoparticles based on Pt−Ni present a potential class of stable and active nanoparticles. Choi et al. reported high activities for Pd@Pt−Ni octahedral nanoparticles with an exceptional durability under ORR conditions.[15]

Li et al. discussed Fe-doped octahedral Pt_3Ni nanocrystals that have a stable octahedral shape after 16 000 potential cycles in acidic media while losing only around 25% of mass activity. However, the mass activities after activation (0.35 A mg_{Pt}^{-1}) already were significantly lower than the one for the bimetallic Pt−Ni octahedral (8x higher) nanocatalyst.[16] Huang et al. recently reported Mo-doped Pt−Ni octahedral nanoparticles with an outstanding ORR performance of 6.98 A mg_{Pt}^{-1} and a loss in activity after 8,000 potential cycles of only 5%.[17] Zhang et al. tried to overcome the problem of limited stability by introducing Cu into the Pt−Ni alloy.[18] Their Pt_2CuNi catalyst showed remarkable high activities of 2.35 A mg_{Pt}^{-1}, a loss of only 19% after 4,000 electrochemical cycles and a retention in shape in acidic media. Recently, Yan et al. discussed cubic and octahedral Pd−Rh alloys with different metal ratios as stable electro-catalysts for the ORR and obtained the lowest mass-activity loss of only 20% in acidic media for the most Rh-rich particles, which consist of 80% Rh and 20% Pd.[17] Although Rh has a negative influence on the initial activity itself (0.12 A mg_{Pt}^{-1}), it significantly improves the stability toward the ORR and does not have negative side effects like iron, which also catalyzes the strongly exothermic decomposition of hydrogen peroxide, a possible side product in ORR, or copper, which could be reduced on the Pt anode and therefore block the surface sites for hydrogen oxidation reaction.[19,20] An active spherical Pt−Rh−Ni system has been reported by Erini et al., which exhibits an exceptionally high activity toward ethanol oxidation in alkaline media.[21]

Herein, we present an investigation of newly designed near-surface Rh-doped Pt−Ni octahedral nanoparticles supported on carbon. This novel catalyst exhibits exceptional shape stability, remarkable high ORR activity and electrochemical stability compared to a Pt−Ni octahedral catalyst. Both catalysts were synthesized using a modified organic phase reduction method, where Rh was added at a later stage of the synthesis protocol to settle Rh mainly on the surface.[10,11,22] To the best of our knowledge, we are first who show that Rh has a beneficial influence on electrochemical and octahedral shape stability of bi- or trimetallic Pt−Ni nanocatalysts, which represents a new class of stable octahedral shaped Pt−Rh−Ni nanoparticles during the electrochemical treatment for the ORR.

Platinum−rhodium−nickel particles with 3 atom % Rh have been synthesized using a solvothermal method with oleylamine and oleic acid as solvents and tungsten hexacarbonyl as reducing and shape directing agent, followed by an acetic acid treatment to purify the particle surface and adjust the noble-metal-to-nickel ratio. The same method was used to synthesize bimetallic Pt−Ni octahedral particles, which are supposed to serve as a comparison and reference. All details on the experimental methods and synthesis are presented in the Supporting Information (SI).

The elemental composition and the Pt-based weight loadings on the carbon support vulcan XC 72R were determined by the use of ICP OES. After acetic treatment (initial), the compositions were $Pt_{81}Ni_{19}$ and $Pt_{71}Rh_3Ni_{26}$ and the Pt-based weight loading was 26 wt % for Pt−Ni/C and 24 wt % for Pt−Rh−Ni/C, respectively.

X-ray powder diffraction patterns for both catalysts show a single face-centered cubic structure (Figure 1). Compared to

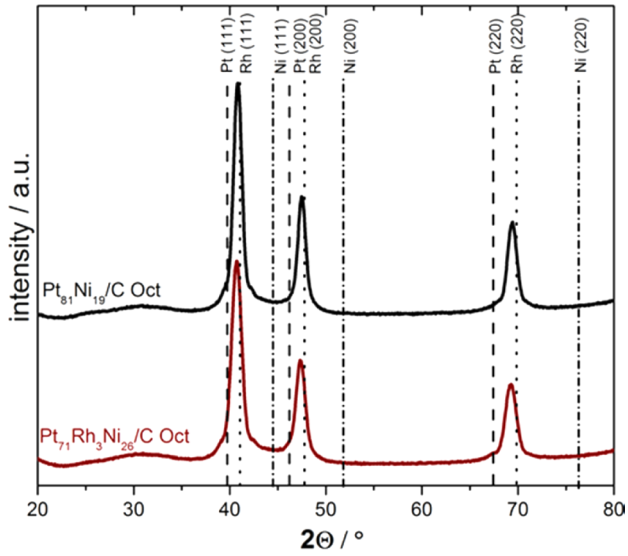

Figure 1. XRD profiles of $Pt_{71}Rh_3Ni_{26}$/C octahedra (red) and $Pt_{81}Ni_{19}$/C octahedra (black). Dashed, dotted, and dashed-dotted lines denote pure Pt (PDF #0802), Rh (PDF #0685), and Ni (PDF #0850) face-centered cubic pattern.

pure Pt reflexes, the reflexes of both samples are shifted to higher 2θ angles due to the decreased lattice constant of the Pt−Ni alloy. With the incorporation of Rh, there is no significant shift in the peak position due to the very small amount of Rh. The theoretical 2θ values match nicely the measured values (see SI, Table S1) using the Vegard's law.

Transmission electron microscopy (TEM) and high-angle annular dark-field (HAADF) scanning transmission electron microscopy (STEM) were used to investigate the particle size and particle distribution on the carbon support. The initial Pt−Rh−Ni particles are well distributed on the carbon support (Figure 2a−d) with an average edge length of 7.4 ± 1.0 nm (see SI, Figure S1a,b). Most particles possess an octahedral shape with rounded corners or are truncated octahedra (red arrows) (Figure 2b,c). Rounded corners likely present an energetically more stable shape than sharp edges and are therefore favored.[23] The Pt−Ni/C catalyst also shows homogeneously distributed octahedral-shaped particles with similar edge length of 7.9 ± 1.1 nm (see SI, Figure S2). Because the particles have different crystallographic orientation with respect to the incident electron beam during TEM inves-

DOI: 10.1021/acs.nanolett.5b04636
Nano Lett. 2016, 16, 1719−1725

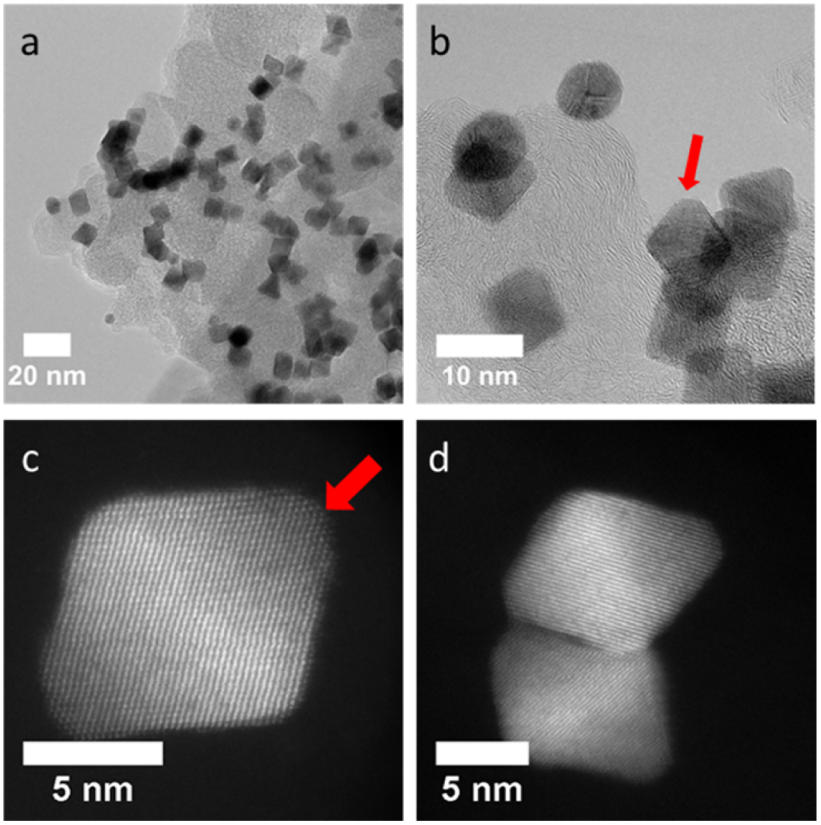

Figure 2. Transmission electron microscopy images of $Pt_{71}Rh_3Ni_{26}/C$ after synthesis and acetic acid treatment. (a) Overview of the particles with a homogeneous distribution; (b) most particles are octahedral with rounded corners or octahedral (red arrow) particles; and (c,d) HAADF STEM images of a truncated octahedron.

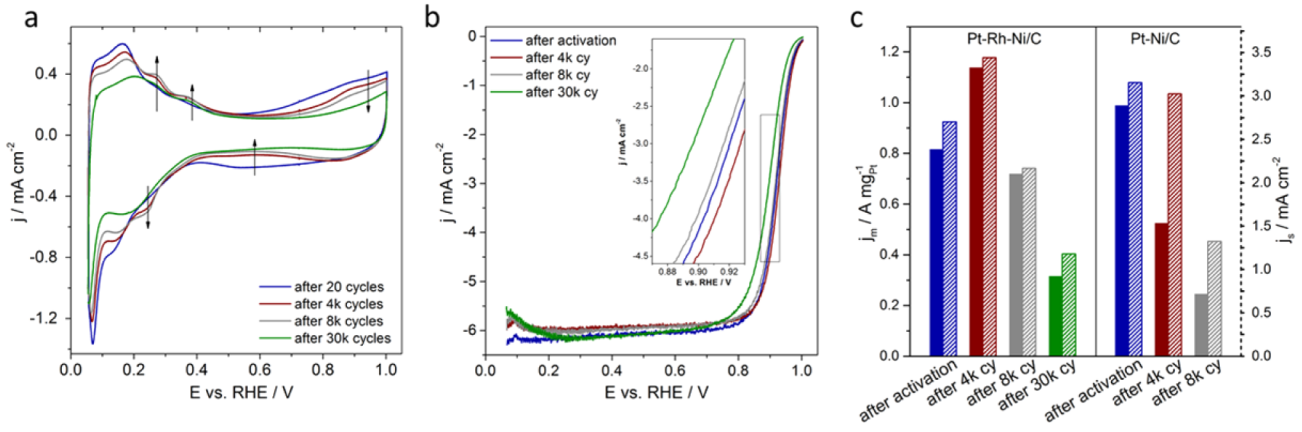

Figure 3. Electrochemical characterization of $Pt_{71}Rh_3Ni_{26}/C$ (iR corrected): a) cyclovoltammograms after 20 cycles (cy) activation, after 4k, 8k and 30k cycles stability test between 0.05−1.0 V vs RHE with 100 mV s^{-1} in N_2 saturated 0.1 M $HClO_4$ electrolyte, 0 rpm (currents normalized on rotating disc electrode area 0.196 cm^2); b) linear sweep voltammetry after a particular number of cycles between 0.05−1.0 V vs RHE with 10 mV s^{-1} in O_2 saturated 0.1 M $HClO_4$ electrolyte, 1600 rpm (currents normalized on rotating disc electrode area 0.196 cm^2); c) mass (solid bars) and specific activity (dashed bars) compared to the bimetallic $Pt_{81}Ni_{19}/C$ oct (evaluated at 0.9 V).

tigation, the true edge length will be slightly different from the one measured in projection.

The electrochemical characteristics of the Pt−Rh−Ni/C catalyst were determined in acidic media (0.1 M $HClO_4$) using a thin-film rotating disk electrode.

Figure 3a shows the cyclic voltammograms of the Pt−Rh−Ni/C catalysts after different numbers of electrochemical cycles. After activation (20 cycles), the catalysts exhibit high current densities in the H_{upd} region as well as in the Pt−OH region, which are decreasing continuously with the number of cycles during electrochemical stability measurements, possibly due to the local changes on the surface of the Pt−Rh−Ni catalysts. These changes are most likely induced by Pt/Rh atomic migration and faceting on the surface.[24] The evaluation of the peak intensities shows a nonmonotonic behavior. After 8k (k = 1000) cycles, peaks at 0.25 and 0.4 V versus RHE in the anodic scan exhibit the largest intensities.

For electrochemical activity measurements, linear sweep voltammetry was performed (Figure 3b). After a stability test involving a defined number of cycles, the positive-going

DOI: 10.1021/acs.nanolett.5b04636
Nano Lett. 2016, 16, 1719−1725

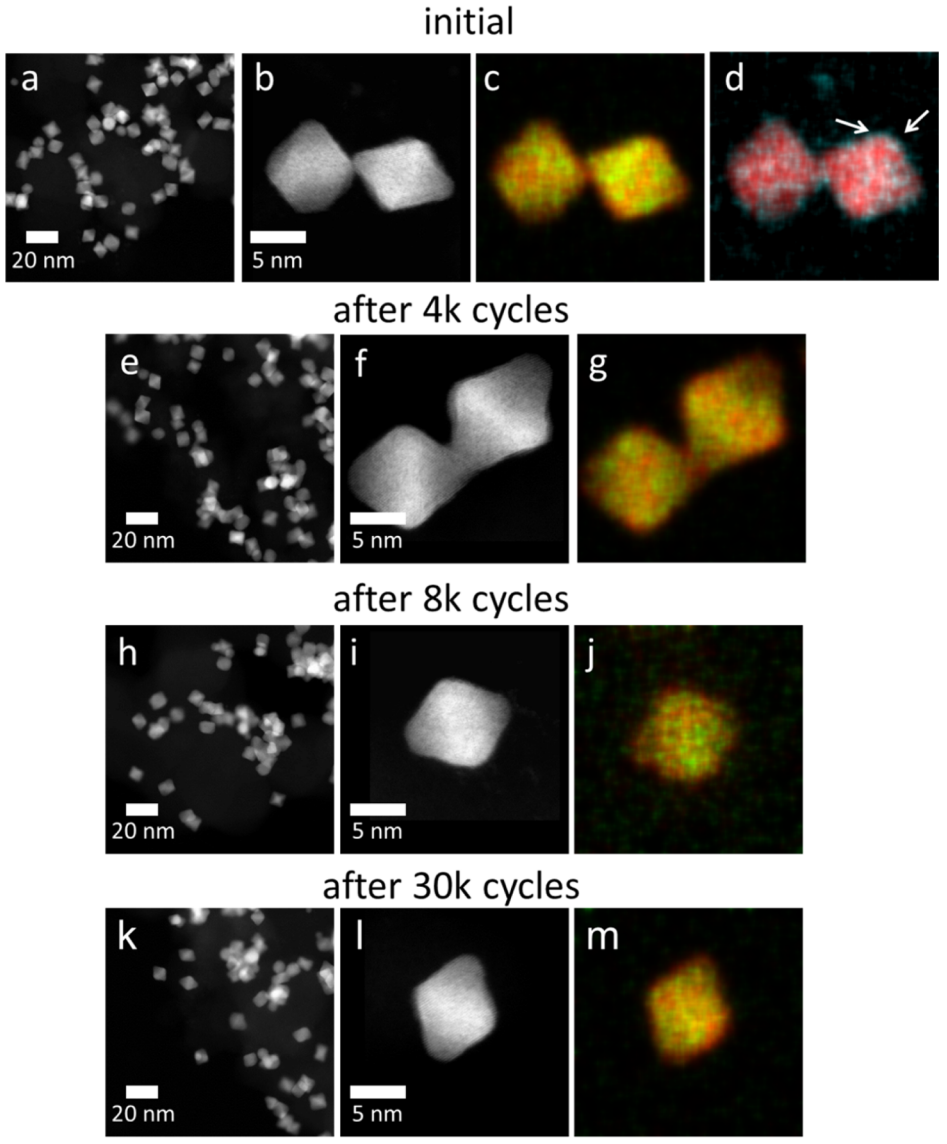

Figure 4. HAADF STEM images and EDX composition maps of Pt−Rh−Ni octahedral nanoparticles. (a,e,h,k) Overview HAADF STEM images of the nanoparticles in the initial state (a), after 4k cycles (e), after 8k cycles (h), and after 30k cycles (k). (b,f,i,l) High-resolution HAADF STEM images of Pt−Rh−Ni octahedral nanoparticles oriented close to ⟨110⟩ in different states. (c,g,j,m) Pt (red) and Ni (green) EDX composition maps and (d) Pt (red) and Rh (blue) EDX composition map of the corresponding octahedral nanoparticles, respectively.

polarization curves for the ORR were recorded in O_2-saturated 0.1 M $HClO_4$ electrolyte and have been evaluated at 0.9 V versus RHE. For Pt−Rh−Ni/C, the mass activity increases from 0.82 A mg_{Pt}^{-1} in activated state to an even higher value of 1.14 A mg_{Pt}^{-1} after 4k cycles and decreases to 0.72 A mg_{Pt}^{-1} after 8k cycles, which is a loss of only 12% compared to the activated state, and to 0.32 A mg_{Pt}^{-1} after 30k cycles. This behavior is surprising, as octahedral Pt−Ni based catalysts with improved mass-based and specific activity after 4k stability cycles are not that common yet.[13,18,25] The Mo-doped Pt−Ni/C octahedral particles reported in literature indeed show significantly higher overall ORR activities after stability tests, but they exhibit a small loss in activity after 4k cycles.[17] Compared to the bimetallic Pt−Ni/C catalyst, the presence of Rh indeed reduces the mass-based activity after activation (0.82 versus 0.99 A mg_{Pt}^{-1}) as mentioned before, but it exhibits a high mass-based activity after 4k cycles (Figure 3c). But the Pt−Ni/C catalyst shows a dramatic mass-based activity drop to 0.30 A mg_{Pt}^{-1} (70%) after 4k cycles and even further after 8k cycles to 0.12 A mg_{Pt}^{-1} (88%). The specific activity based on the electrochemical surface area (ECSA) determined by H_{upd} (see SI, Figure S3 b,c) follows the same trend. For comparison, we synthesized particles with an even smaller Rh amount than 3 atom %, $Pt_{73}Rh_1Ni_{26}$ and $Pt_{72}Rh_2Ni_{26}$. Anyway, these amounts were too small to improve the electrochemical long-term stability, but the mass-based activities after activation were slightly higher than for the 3 at % Rh-modified catalyst (see SI, Figure S3a). This is in good accordance with the high activity of the bimetallic octahedral Pt−Ni/C after activation. Thus, we conclude that in the investigated range of Rh contents, Rh slightly reduces the ORR activity after activation but dramatically enhances the electrochemical long-term stability. We hypothesize the existence of the optimum Rh content for high activity and stability values for Pt−Ni octahedral-shaped nanoparticles.

Comparing the cyclic voltammograms of the most active state of Pt−Ni/C (after 20 cycles activations) and Pt−Rh−Ni/C (after 4k cycles stability test), both catalysts seem to exhibit a

DOI: 10.1021/acs.nanolett.5b04636
Nano Lett. 2016, 16, 1719−1725

comparable surface structure in terms of hydrogen adsorption and desorption features in these states after electrochemical treatment (see SI, Figure S4). CO-oxidation experiments have been performed to get more detailed information on the surface characteristics of the initial and activated Pt−Rh−Ni/C (see SI, Figure S5). The early CO-oxidation peak at 0.45 V versus RHE before and after activation indicates an oxygen donation species on the surface, which is even more pronounced after 20 cycles electrochemical activation. Hence, a Rh species on or directly below the surface can be proposed.

To understand these electrochemical observations we utilized a detailed TEM-investigation in combination with HAADF STEM and energy dispersive X-ray (EDX) to investigate the Pt−Rh−Ni/C catalyst after different stages of the electrochemical cycles stability test. Figure 4 shows the respective HAADF STEM images and EDX composition maps. The HAADF images of the initial catalyst, that is, after synthesis and acid leaching, as well as the same catalyst after 4k, after 8k, and after 30k cycles exhibit well-distributed particles on the carbon support exhibiting mainly octahedral shape (Figure 4a,b,e,f,-a,b,e,f,h,i,k,l). The retention of the octahedral shape after 8k cycles and especially after 30k cycles was unexpected because the octahedral shape for the Pt−Ni/C catalyst disappears already after 4k stability cycles. In fact, for Pt-rich octahedral Pt−Ni nanoparticles a loss in shape was reported.[13,14] Also in direct comparison with our bimetallic Pt−Ni/C catalyst a loss in shape, especially after 8k cycles stability test (see SI, Figures S6 and S7) could be observed, while the Pt−Rh−Ni/C catalyst still has an octahedral shape.

The corresponding EDX composition maps of the Rh-doped Pt−Ni particles are shown in Figure 4c,d,g,j,m. In the initial state, the EDX map of two octahedral nanoparticles oriented close to the ⟨110⟩ zone axis, indicates a Pt-rich frame, which is pointed out by a Pt-rich strip in the middle of the nanoparticles (Figure 4c) and an enrichment of Ni at the ⟨111⟩ facets. This elemental distribution is absolutely comparable with our previous work.[13,14] Furthermore, Rh is accumulated at the surface of the particles (in Figure 4d highlighted by arrows and additionally shown in Figure S8), which is in good accordance with the results of the CO-stripping experiment. EDX quantification yields a composition of Pt 69 atom %, Ni 25 atom %, and Rh 6 atom % of the nanoparticles imaged in Figure 4b and an average composition of Pt 69 atom %, Ni 26 atom %, and Rh 5 atom % of particles in the initial state. It should be mentioned at this point that our EDX composition analyses of the initial particles are corresponding very well with the results obtained by the ICP OES analysis ($Pt_{69}Rh_5Ni_{26}$ versus $Pt_{71}Rh_3Ni_{26}$). Thus, it is reasonable to assume that even if EDX is limited locally, the obtained compositions are right.

After 4k cycles, EDX quantification yields an average composition of Pt 74 atom %, Ni 24 atom %, and Rh 2 atom %. The composition of Pt 76 atom %, Ni 24 atom %, and Rh 0 atom % was found for the nanoparticles imaged in Figure 4f. These results indicate that Rh is partially dissolved from the surface during the first 4k cycles. The error of measurement of the EDX quantification was determined as ±2 atom %, hence the concentration of Rh is at the limit of detection by EDX. The EDX composition map in Figure 4g shows a similar distribution of Pt and Ni comparable to the initial sample, i.e. an enrichment of Ni at the facets and a Pt-rich frame. Furthermore, Pt is observed at the outermost parts of the octahedra, which due to the projection along a ⟨110⟩ direction are likely caused by the presence of Pt-rich edges or the formation of a thin Pt-rich skin on the facets of the octahedra.

After 8k cycles, the octahedral shape is still retained; however the typical Pt-rich strip is not visible, rather Ni seems to be distributed in the center of the octahedron as well (Figure 4j). This observation indicates that the segregated structure, showing a Pt frame and Ni at the facets observed in the initial and 4k cycled particles, is dispersed toward a more homogeneously alloyed nanoparticle structure. The outermost parts of the octahedron are again Pt-rich.

The same is true after 30k cycles: The particles retain an octahedral shape, the outermost parts are Pt-rich and the innermost parts are essentially homogeneously alloyed without showing significant segregation (Figure 4m). The average composition after 8k and 30k cycles is Pt 74 atom %, Ni 25 atom %, Rh 1 atom %, and Pt 74 atom %, Ni 25 atom %, Rh 1 atom %, respectively. No significant change of the composition, especially of the Ni-content, is observed after long-term cycling.

In addition to our standard electrochemical stability measurements between 0.5 and 1.0 V versus RHE, following the DOE target,[26] we also performed a series of durability measurements between 0.6 and 1.2 V versus RHE. The EDX composition analyses are reported in the SI (see Figure S9 and S10) and show nanoparticles with octahedral shape even after 30k cycles under this condition.

In order to study the influence of Rh on the structural evolution during cycling, we investigated Pt−Ni octahedral nanoparticles in the initial state and after 4k and 8k cycles (see SI, Figure S7). While the EDX composition map of the initial state as well as the 4k state shows a similar distribution of Pt and Ni compared to the Pt−Rh−Ni catalyst (see SI, Figure S7c,f), the octahedral shape is lost after 8k cycles and the particles become nearly spherical (see SI, Figure S7g). The EDX map demonstrate that a Pt-rich shell is build up around the Pt−Ni alloy spherical particle (see SI, Figure S7i). The average composition of the Pt−Ni particle in the initial state, after 4k, and after 8k cycles is Pt 79 atom %, Ni 21 atom %, Pt 78 atom %, Ni 22 atom %, and Pt 77 atom %, Ni 23 atom %, respectively.

Hence, no significant compositional change is observed either for this catalyst. The stable Ni content during stability measurements seems contradictive to similar Pt−Ni alloy systems discussed previously.[4,13] The reason why Ni is not leached out is probably because the particles were treated in acetic acid after synthesis. Thereby a Pt−Rh shell was built that seems to be thick enough to protect Ni from further leaching. Rh, which is mainly located near the surface, is rather leached out in the electrochemical treatment as its redox potential is at 0.600/0.758 V versus RHE,[27] which lies directly in the potential window of the electrochemical stability tests. It is undergoing a permanent oxidation/reduction procedure and therefore stays close to the outermost layer of the Pt−Ni−Rh nanocatalyst. Therefore, it is plausible to assume that Ni is protected by a Pt shell on the particle surface.

On the basis of the composition analyses, we also conclude that the loss in shape and activity of the Pt−Ni/C nanoparticles and the loss in activity of the Pt−Rh−Ni/C nanoparticles are not related to the dissolution of Ni but rather to the segregation of Pt and Ni.

For Pt−Ni/C, the loss in activity is obviously caused by the loss in shape, which is not true for Pt−Rh−Ni/C. In order to explain the decrease in activity for the Pt−Rh−Ni/C, we note the change in anisotropy with increasing cycles (Figure 4). In

DOI: 10.1021/acs.nanolett.5b04636
Nano Lett. 2016, 16, 1719−1725

particular, Ni segregation at the facets and Pt at the edges have proved to be favorable for high catalytic ORR activities,[13,14,28] but this distribution is not evident after 8k and especially after 30k cycles. Although high catalytic activities and durability are significantly influenced by the stability of the octahedral shape associated with the presence of active surface facets (compared to Pt−Ni/C after 8k cycles in this study), the presence of a favorable surface composition (anisotropy of Ni and Pt, compared to Pt−Rh−Ni/C after 8k cycles) is also necessary in order to achieve high catalytic activity. Therefore, we hypothesize that the catalytic activity loss during the durability test is mostly caused by the loss of favorable Ni segregation at the facets of octahedral shaped nanoparticles and not only by the octahedral-shaped entity.

The diffusion behavior of the Pt atoms during electrochemical potential cycling seems to be affected by the presence of Rh. Because Rh is mainly located at the surface of the particles, it seems to suppress diffusion of Pt at the edges and kinks resulting in a stable shape even after 30k electrochemical cycles. Therefore, a small amount of Rh on the surface seems to be sufficient to keep the octahedral shape, however, it is unable to stabilize anisotropy. A possible explanation for the ability of Rh to change the Pt segregation behavior was given by Zhang et al., who suggested, based on density functional theory calculations, that some transition metals M, doped on a Pt_3Ni/M (111) surface are able to promote or suppress Pt segregation to the surface.[29] On the basis of Pt surface segregation energies, Rh, in comparison to Ni, exhibits more positive values suggesting suppressing Pt segregation rather than Ni. More broadly, our study suggests that Rh-doped Pt alloy surfaces can be a general strategy to stabilize octahedral nanoparticle surfaces.

In conclusion, we design and present a synthetic pathway for near-surface Rh-doped Pt−Ni catalysts with well-defined shapes using a solvothermal method. The resulting Pt−Rh−Ni particles were tested for the electrochemical ORR and exhibit an exceptional and improved activity and stability behavior. Compared to a bimetallic Pt−Ni/C catalyst, the activity after 4k cycles electrochemical stability test is improved and the octahedral shape remained nearly unaffected even after 30k cycles. In contrast, the reference Pt−Ni octahedral particles lost around 70% of their initial activity already after 4k cycles and completely lost their shape after 8k cycles. These observations are explained by detailed microstructural investigations of the atomic rearrangement processes on the surfaces of the two catalysts. It was found that the shape losses occur mainly due to the Pt atom diffusion during dynamic potential cycling and Rh suppresses the diffusion of Pt atoms. Therefore, small amounts of Rh prevent a loss in shape and maintain active surface structures and particle shapes during and after the electrochemical treatment. In conclusion, these results could serve as a guideline for a new class of active and stable-shaped electrocatalysts.

■ ASSOCIATED CONTENT

Supporting Information

The Supporting Information is available free of charge on the ACS Publications website at DOI: 10.1021/acs.nanolett.5b04636.

Experimental details, table of 2θ XRD values, TEM images, HAADF STEM images and EDX compositions maps, graphics of particle size distribution, bar charts of electrochemical evaluation, comparison of cyclic voltammograms, and CO stripping voltammograms. (PDF)

■ AUTHOR INFORMATION

Corresponding Author

*Email: pstrasser@tu-berlin.de.

Notes

The authors declare no competing financial interest.

■ ACKNOWLEDGMENTS

We thank the Zentraleinrichtung für Elektronenmikroskopie (ZELMI) of the Technical University Berlin and Manuel Gliech for its support with TEM measurements. Financial support was given by Deutsche Forschungsgemeinschaft (DFG) Grants STR 596/5-1 ("Shaped Pt bimetallics") and HE 7192/1-1. P.S. acknowledges partial funding by the German Federal Ministry of Education and Research (Bundesministerium für Bildung und Forschung, BMBF) under Grant "LOPLAKAT".

■ REFERENCES

(1) Gasteiger, H. A.; Markovic, N. M. *Science* **2009**, *324* (5923), 48−49.
(2) Duan, Z.; Wang, G. *Phys. Chem. Chem. Phys.* **2011**, *13* (45), 20178−20187.
(3) Stamenkovic, V.; Mun, B. S.; Mayrhofer, K. J. J.; Ross, P. N.; Markovic, N. M.; Rossmeisl, J.; Greeley, J.; Nørskov, J. K. *Angew. Chem.* **2006**, *118* (18), 2963−2967.
(4) Gasteiger, H. A.; Kocha, S. S.; Sompalli, B.; Wagner, F. T. *Appl. Catal., B* **2005**, *56*, 9−35.
(5) Gan, L.; Heggen, M.; Rudi, S.; Strasser, P. *Nano Lett.* **2012**, *12* (10), 5423−5430.
(6) Gan, L.; Cui, C.; Rudi, S.; Strasser, P. *Top. Catal.* **2014**, *57* (1−4), 236−244.
(7) Oezaslan, M.; Strasser, P. *J. Power Sources* **2011**, *196* (12), 5240−5249.
(8) Hasche, F.; Oezaslan, M.; Strasser, P. *ChemCatChem* **2011**, *3* (11), 1805−1813.
(9) Stamenkovic, V. R.; Fowler, B.; Mun, B. S.; Wang, G. F.; Ross, P. N.; Lucas, C. A.; Markovic, N. M. *Science* **2007**, *315* (5811), 493−497.
(10) Zhang, J.; Yang, H.; Fang, J.; Zou, S. *Nano Lett.* **2010**, *10*, 638.
(11) Choi, S.-I.; Xie, S.; Shao, M.; Odell, J. H.; Lu, N.; Peng, H.-C.; Protsailo, L.; Guerrero, S.; Park, J.; Xia, X.; Wang, J.; Kim, M. J.; Xia, Y. *Nano Lett.* **2013**, *13* (7), 3420−3425.
(12) Choi, S.-I.; Xie, S.; Shao, M.; Lu, N.; Guerrero, S.; Odell, J. H.; Park, J.; Wang, J.; Kim, M. J.; Xia, Y. *ChemSusChem* **2014**, *7* (5), 1476−1483.
(13) Cui, C.; Gan, L.; Heggen, M.; Rudi, S.; Strasser, P. *Nat. Mater.* **2013**, *12* (8), 765−771.
(14) Gan, L.; Cui, C.; Heggen, M.; Dionigi, F.; Rudi, S.; Strasser, P. *Science* **2014**, *346* (6216), 1502−1506.
(15) Choi, S.-I.; Shao, M.; Lu, N.; Ruditskiy, A.; Peng, H.-C.; Park, J.; Guerrero, S.; Wang, J.; Kim, M. J.; Xia, Y. *ACS Nano* **2014**, *8* (10), 10363−10371.
(16) Li, Y.; Quan, F.; Chen, L.; Zhang, W.; Yu, H.; Chen, C. *RSC Adv.* **2014**, *4* (4), 1895−1899.
(17) Huang, X.; Zhao, Z.; Cao, L.; Chen, Y.; Zhu, E.; Lin, Z.; Li, M.; Yan, A.; Zettl, A.; Wang, Y. M.; Duan, X.; Mueller, T.; Huang, Y. *Science* **2015**, *348* (6240), 1230−1234.
(18) Zhang, C.; Sandorf, W.; Peng, Z. *ACS Catal.* **2015**, *5* (4), 2296−2300.
(19) Lin, S.-S.; Gurol, M. D. *Environ. Sci. Technol.* **1998**, *32* (10), 1417−1423.
(20) De Laat, J.; Gallard, H. *Environ. Sci. Technol.* **1999**, *33* (16), 2726−2732.
(21) Erini, N.; Rudi, S.; Beermann, V.; Krause, P.; Yang, R.; Huang, Y.; Strasser, P. *ChemElectroChem* **2015**, *2* (6), 903−908.

DOI: 10.1021/acs.nanolett.5b04636
Nano Lett. 2016, 16, 1719−1725

(22) Kang, Y.; Pyo, J. B.; Ye, X.; Diaz, R. E.; Gordon, T. R.; Stach, E. A.; Murray, C. B. *ACS Nano* **2013**, *7* (1), 645−653.
(23) Alpay, D.; Peng, L.; Marks, L. D. *J. Phys. Chem. C* **2015**, *119* (36), 21018−21023.
(24) Grozovski, V.; Solla-Gullon, J.; Climent, V.; Herrero, E.; Feliu, J. M. *J. Phys. Chem. C* **2010**, *114* (32), 13802−13812.
(25) Rudi, S.; Tuaev, X.; Strasser, P. *Electrocatalysis* **2012**, *3* (3−4), 265−273.
(26) U.S. Department of Energy. *Multi-Year Research, Development and Demonstration Plan*; 2012. http://energy.gov/sites/prod/files/2014/12/f19/fcto_myrdd_fuel_cells.pdf (accessed Dec 18, 2015).
(27) Vanysek, P. CRC Press LLC: Boca Raton, 2000. http://downloads.gphysics.net/UACh/Medicina/TablasIones.pdf (accessed Feb 11, 2016).
(28) Arán-Ais, R. M.; Dionigi, F.; Merzdorf, T.; Gocyla, M.; Heggen, M.; Dunin-Borkowski, R. E.; Gliech, M.; Solla-Gullón, J.; Herrero, E.; Feliu, J. M.; Strasser, P. *Nano Lett.* **2015**, *15* (11), 7473−7480.
(29) Zhang, Y.; Duan, Z.; Xiao, C.; Wang, G. *Surf. Sci.* **2011**, *605* (15−16), 1577−1582.

DOI: 10.1021/acs.nanolett.5b04636
Nano Lett. 2016, 16, 1719−1725